Original Paper Open Access

Combined approaches provide an anatomical and transcriptomic fingerprint of maize cell wall digestibility

Mary S-J Wong Quai Lam[1,2], Yves Martinez[1,3], Odile Barbier[1,2], Alain Jauneau[1,3], Sandrine Balzergue[4], Stéphanie Huguet[4], Brigitte Pollet[5], Valérie Méchin[5], Fabienne Guillon[6], Paul Robert[6], Claire Dumon[7,8,9], Michael O'Donohue[7,8,9], Deborah Goffner[1,2], Magalie Pichon[1,2]*

[1]Université de Toulouse, UPS, UMR5546, Laboratoire de recherche en Sciences Végétales, BP42617, F-31326 Castanet-Tolosan CEDEX, France
[2]CNRS, UMR5546, BP 42617, 31326 Castanet-Tolosan cedex, France
[3]CNRS, FR3450, BP42617, 31326 Castanet-Tolosan cedex, France
[4]INRA - CNRS - URGV, 2 rue Gaston Crémieux, CP5708, 91057 Evry cedex, France
[5]INRA, AgroParisTech, Institut Jean-Pierre Bourgin, UMR1318, 78026 Versailles, France
[6]INRA, UR1268 Biopolymères, Interactions, Assemblages, 44316 Nantes, France
[7]INRA, UMR792 Ingénierie des Systèmes Biologiques et des Procédés, 31400 Toulouse, France
[8]Université de Toulouse; INSA, UPS, INP, LISBP, 135 Avenue de Rangueil, 31077 Toulouse, France
[9]CNRS, UMR5504, 31400 Toulouse, France
*Corresponding author: E-mail: magalie.pichon@toulouse.inra.fr

Abstract

Understanding cell wall biosynthesis and degradation in grasses has become a major aim in plant biology. Although independent previous reports have focused on specific features that dictate cell wall digestibility, cytological, biochemical, and gene regulation parameters have never been integrated within the same study. Herein, we applied a combination of state-of-the-art technologies and different scales of observation on two maize lines that are characterized by highly contrasted forage digestibility. Comparative image analysis of internode sections allow to get an anatomical fingerprint associated with high digestibility: a thin peripheral rind of lignified parenchyma, small numerous vascular bundles, and low proportion of PeriVascular Sclerenchyma (PVS). This cell type patterning led to enhanced digestibility when internode sections were treated with Celluclast, a commercially cell wall degrading enzyme. At a lower scale of observation, Laser Capture Microdissection (LCM) followed by thioacidolysis of PVS revealed a higher proportion of Syringyl (S) unit lignins in the low digestible line while the high digestible line was p-Hydroxyphenyl (H)-rich. Moreover, cytological observation of internodes of the two lines point out that this difference in composition is associated with a delayed lignification of PVS. At the same time, comparative transcriptomics on internodes indicated differential expression of several genes encoding enzymes along the phenylpropanoid pathway and known cell wall-associated Transcription Factors (TFs). Together, these results give an integrative view of different factors which could aim in designing a maize silage ideotype and provide a novel set of potential regulatory genes controlling lignification in maize.

Keywords: cell wall, digestibility, Fourier-transformed infrared (FTIR), gene expression, Laser Capture Microdissection (LCM), stem anatomy, Zea mays

Introduction

Whole plant digestibility is an important trait for silage maize breeding of genotype with higher feeding value. However, understanding why a given maize line is more or less digestible at the whole plant level is not an easy task due to the multiplicity of lignified cell types, each presumably with a specific cell wall composition and structure. For example, in a transverse section of a maize internode, the peripheral rind region contains 2-3 Sub-Epidermal layers of lignified Sclerenchyma cells (SES), numerous and closely-spaced Vascular Bundles (VB) composed of lignified vessels embedded in PeriVascular Sclerenchyma (PVS) and lignified parenchyma tissue. In the central pith region, vascular bundles are less numerous and the parenchyma cells are not lignified. Typically, cell wall chemistry and digestibility estimates are performed on ground internode samples and consequently, the data represent average amounts of each compound without taking into account the relative proportions of the different cell types. That said, correlations between stem anatomy and digestibility have been reported in different grasses such as sorghum (Schertz and Rosenow, 1977; Wilson, 1993), barley (Cherney et al, 1990; Goto et al, 1991) and switchgrass (Twidwell et al, 1990). In maize, a study of 22 lines indicated a positive correlation between the total surface area of lignified tissues and digestibility (Mechin et al, 2005). At the same time, Boon et al (2005) could not strictly correlate internode anat-

 RECEIVED 06/26/2013

omy and digestibility in in vitro rumen fermentation studies on two maize lines of contrasted digestibility. Thus, in maize, a detailed picture of the correlation between lignified cell type patterning and digestibility is not yet well established.

In an attempt to determine the relative degradability of the different cell types in maize, Lopez et al (1993), showed that mechanically isolated parenchyma devoid of secondary wall thickenings were more susceptible to degradation by cellulase than sclerenchyma cells. Scanning Electron Microscopy (SEM) studies confirmed a higher digestibility of parenchyma compared to sclerenchyma when subjected to rumen microbial degradation (Migné, 1995). Moreover, for a given cell type, the authors observed differences in digestibility in the upper vs the lower portions of an internode within a genotype, but they were not able to distinguish between lines of contrasted digestibility.

Although the aforementioned studies are of great interest, it is now possible to revisit digestibility with recently developed technologies that probe cell wall chemistry at the cellular level. Fourier-transformed infrared (FT-IR) microspectroscopy allow to detect a broad range of alterations in cell wall structure and architecture (Sindhu et al, 2007) and has been used for high through-put screening to identify novel cell wall mutants (McCann et al, 2007; Mouille et al, 2003). Within the last decade, Laser Capture Microdissection (LCM) has been employed to obtain cell type-specific gene expression (Dembinsky et al, 2007; Nakazono et al, 2003) and proteomic (Dembinsky et al, 2007) data in maize. More recently, LCM has also been used to obtain cell type-specific cell wall chemistry in *Medicago sativa* and *Arabidopsis thaliana* (Nakashima et al, 2008; Ruel et al, 2009). For example, thioacidolysis performed on micro-dissected tissues unequivocally proved that interfascicular fibers of Arabidopsis display a higher Syringyl (S) /Guaiacyl (G) ratio compared to vascular bundles (Ruel et al, 2009).

Several independent gene expression studies in association with maize digestibility have been reported. For example at the single gene level, down-regulated Caffeic acid O-methyltransferase (COMT) and Cinnamoyl-CoA Reductase (CCR) maize plants exhibited significantly higher digestibility and a modified lignin composition that could be related to a re-orientation of the phenylpropanoid pathway (Guillaumie et al, 2007a; Tamasloukht et al, 2011). Transcriptomic studies performed on four different brown-midrib (bm) maize mutants, all known for their higher digestibility, indicated that despite a similar bm phenotype, these mutants exhibited specific transcriptomic fingerprints (Guillaumie et al, 2007a). For example, the *bm1* mutation in Cinnamyl Alcohol-Dehydrogensase (CAD) resulted in lower levels of gene expression of number of the CAD family members. Comparative transcriptomics have also been performed on recombinant inbred lines to study the effect of a major QTL that explains 40% of digestibility (Thomas et al, 2010; Courtial et al, 2012). Although this is an elegant approach, this study did not allow the authors to identify specific transcriptional de-regulated genes underlying the QTL, but rather more global changes in the expression of genes dispersed throughout the genome. To date, transcriptomic approaches have never been performed at the genome scale by comparing two lines with different genetic backgrounds and exhibiting highly contrasted digestibility.

As cell wall digestibility properties are complex and multifactor, we developed integrative approaches including cytology, biochemistry, transcript profiling, FTIR and LCM on two contrasted maize lines, F98902 and Cm484. At the whole plant level, F98902, the less digestible line, had the highest lignin content and was enriched in S units. On the contrary, Cm484, the more digestible line, was significantly less lignified and was characterized by a high proportion of H units. At a cellular scale, histochemical observations revealed noticeable differences in morphological and anatomical traits, as well as differences in the timing of lignification of PVS deposition between the two lines. FTIR and LCM technologies highlight significant differences in chemical composition between PVS of the two lines. In attempting to relate genotype to phenotype, transcriptomic data allowed to identify phenylpropanoid and related Transcription Factors (TFs) network associated with low or high cell wall digestibility.

Materials and Methods

Plant growth conditions

Cm484 and F98902 were selected among a panel of maize lines based on preliminary data indicating high and low digestibility respectively (Méchin et al, 2005). Cm484 and F98902 maize lines were grown in greenhouse conditions in pots containing a mixture of compost and fertilizer (Fertil Top Cote) under drip irrigation twice a day (about 4 l h^{-1}). Twice a week, plants were drip irrigated with fertilizers for the whole day. Greenhouse conditions were as follows: 400W sodium lights; temperature between 25° to 28°C. Plants were harvested when they had seven expanded leaves (referred to as piled-up internode at 7-leaf stage), at flowering, or one month after flowering. Internode samples included the basal internode (INternode above Soil, INS) and the internode just below the node bearing the ear (INternode under Ear, INE). Nodes and leaf sheaths were eliminated before analysis.

Lignin and digestibility analysis

Klason lignin, thioacidolysis and digestibility measurements were performed on samples at 7-leaf and flowering (INEs) stages according to the protocols described in Tamasloukht et al (2011). Thioacidolysis of micro-dissected PVS was performed as follows: the PVS was collected on an adhesive cap and carefully detached and transferred into a microcentrifuge tube containing 200 µl of water. The microcentrifuge tube

Table 1 - Agrophysiological traits of Cm484 and F98902 lines grown in greenhouse conditions. The mean values and standard deviations have been calculated from measurements on 15 plants. Assays have been performed during two successive years (2008-2009).

Lines	Height at flowering stage (cm)	Number of IN	Length of INE (cm)	Diameter of INE (cm)	Number of days to flowering
Cm484	136.9 ± 25.0	11 ± 1.5	14.3 ± 2.8	1.5 ± 0.4	60
F98902	183.0 ± 13.3	15 ± 0.6	17.4 ± 2.7	1.6 ± 0.2	75

Number of days to flowering is estimated as the number of days between sowing and male flowering stage when the tassel is fully emerged and at the beginning of pollen shed. (IN: INternode. INE: INternode under Ear).

was washed several times to transfer samples in the thioacidolysis tube. The samples were freeze-dried overnight before the addition of 50 µl of thioacidolysis reagent (C19H40), together with 0.02 µg μl^{-1} of C19H40 and C21H44 (internal standards), that is 1µg per sample. The thioacidolysate was concentrated to a volume of 100 µl. 50 µl of the concentrated thioacidolysate was sampled, dried under liquid nitrogen and silylated with 50 µl of N, O-bis-trimethylsilyl-trifluoroacetamide and 50 µl of pyridine. 1 µl of the solution was injected, by an injector operating at 280°C in the split/splitless mode, onto a Cpg-sm Saturne 2100 (Varian), equipped with a Sulpeco (Saint-Germain-en-Laye, France) SPB1 column (30 m in length x 0,25 mm of internal diameter), operated in the temperature program mode (from 40°C to 180°C at 30°C min^{-1}; then 180°C to 260°C at 2°C min^{-1}; and an isothermal temperature of 260°C). The mass spectral analyses were run with an ion trap (electronic impact, 70 eV). All analyses were carried out as three replicates injection analyses. The determination of the three lignin-derived monomers, H, G and S, were carried out on ion chromatograms at m/z 239, 269 and 299.

Carbohydrate analysis

Neutral sugars were quantified by HPAEC-PAD analysis on samples collected at 7-leaf and flowering (INEs) stages. Briefly, 10 mg of dry matter were incubated in 12 M sulphuric acid for 1 hour at 30°C then sample were diluted in 4% sulphuric acid and hydrolysed during one hour at 120°C. All samples were cooled, diluted, and filtered (PTFE, 0.22 lm) before injection on CarboPac PA-1 column (4 x 250 mm, Dionex). Elution of monosaccharides was obtained with a NaOH–sodium acetate gradient as previously described (Beaugrand et al, 2004). Analytical grade standards of L-arabinose, D-galactose, D-glucose, and D-xylose were used to quantify the concentration of sugars.

Lignin histochemical staining

100 µm thick internode sections were made, from INEs and INSs at flowering and one-month after flowering stages, with a vibratome (LEICA VT 1000S) and stained with phloroglucinol for 30 seconds (Nakano and Meshitsuka 1992). Sections were observed using an inverted microscope (Leitz DMRIBE, Leica Microsystems, Wetzlar, Germany) and images were registered using a CCD camera (Color Coolview, Photonic Science, Milham, UK).

Quantitative measurements of lignified cell types

To calculate the relative proportion of the different cell types, 2 portions of INS sections (100 µm thick) from three plants at flowering stage were stained with phloroglucinol and scanned (6400 dpi). Each tissue type was manually delimited and the surface area of each one was calculated with Image PRO-Plus software (Media Cybernetics, Silver Spring, MD). To evaluate the size distribution of vascular bundles, measurements were performed as described in Tamasloukht et al (2011).

Morphometric characteristics of PeriVascular Sclerenchyma (PVS)

Measurements of the Vascular Bundles (VB) in the rind were performed on 130 µm thick phloroglucinol stained cross-sections of INS at flowering stage. The PVS was manually delimited for the measurement of cell wall density and cell surface area. For each VB in the rind, the total surface area and the lumen area of PVS were calculated using the Image PRO-Plus software (Media Cybernetics, Silver Spring, MD). The relative cell wall area was calculated by subtracting the lumen area from total surface area. Cell wall thick-

Table 2 - Digestibility, lignin content and composition of Cm484 and F98902 internodes at two developmental stages. Each value represent the mean of two assays with individual values varying by < 3% from the mean.

Stage and samples	Lines	Digestibility (IVNDFD) (%)	Klason lignin (%)	Thioacidolysis yield (µmol g^{-1} KL)	Relative frequency of thioacidolysis monomers (Mole %)			S/G
					H	G	S	
Piled-up internodes at 7-leaf stage								
	Cm484	62.67	8.48	415.34	4.65	52.58	42.77	0.81
	F98902	59.83	9.54	420.98	2.88	52.39	44.73	0.85
INE at flowering								
	Cm484	30.12	13.91	710.93	4.09	41.25	54.66	1.32
	F98902	12.85	16.83	641.25	1.90	36.68	61.42	1.67

H: p-hydroxyphenyl; G: guaiacyl; S: syringyl. IVNDFD: In Vitro Neutral Detergent Fiber Digestibility (Méchin et al, 2005); INE : INternodes under Ear

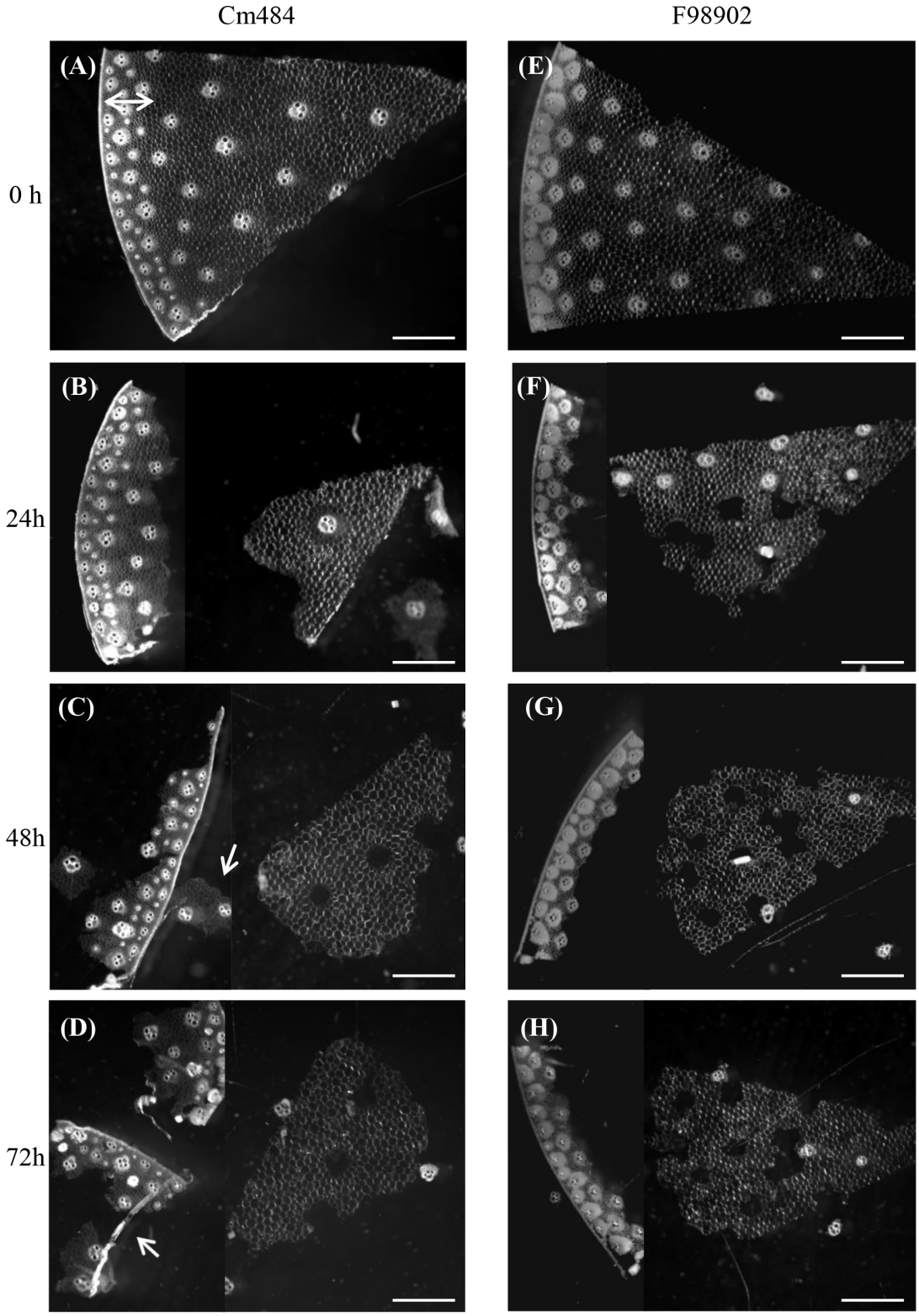

Figure 1 - In section enzymatic degradation of Cm484 and F98902 internodes. **a-d**: 100 μm cross sections of Cm484 were incubated with commercial Celluclast for 24h to 72h. **e-h**: 100 μm cross sections of F98902 were also incubated with commercial Celluclast for 24 to 72h. Double arrows indicate the rind in **a**. Arrows indicate patches of rind parenchyma in **e** and remaining VB and SES after parenchyma degradation in **g**. The degradation was carried out at a temperature of 40°C on three independent internodes (INE) collected at flowering stage for each line. Bars : 2 mm.

ness was measured between two adjacent cells exhibiting the same size. A total of 100 measurements were realized to determine cell wall thickness.

In section enzymatic cell wall hydrolysis

Enzymatic hydrolysis was carried out using cellulase from *Trichoderma reesei* ATCC 26921, with a manufacturer-stated activity of 700 endoglucanase units (EGU)/g (SIGMA-ALDRICH, C2730, Steinheim, Germany). The enzyme was prepared in 500 mM sodium acetate buffer at pH 5.0 and used at a dilution of 1/100. Hydrolysis was performed on 100µm thick cross-sections from INEs at flowering stage. The cross-sections were placed in 1 ml of the enzymatic solution and incubated at 40°C. After 24h, 48h, and 72h, samples were removed from the incubator for observations.

Affymetrix array hybridization

RNA was extracted from 6 INEs collected at the flowering stage, and pooled into two samples for analysis. Hybridization experiments were performed as described in (Cossegal et al, 2008). All raw and normalized data are available through the CATdb database (Gagnot et al, 2008) and from the Gene Expression Omnibus (GEO) repository at the National Center for Biotechnology Information (NCBI) (Barrett et al, 2007) accession number : GSE 18857.

Fourier-Transformed InfraRed spectroscopy (FTIR)

Infrared spectra were collected between 1800 and 800 cm^{-1} at 4 cm^{-1} intervals using a spectrometer (Tensor 27, Bruker) coupled with a microscope (Hyperion 2000, Bruker). Each spectrum resulted from the co-addition of 500 scans. The microscope

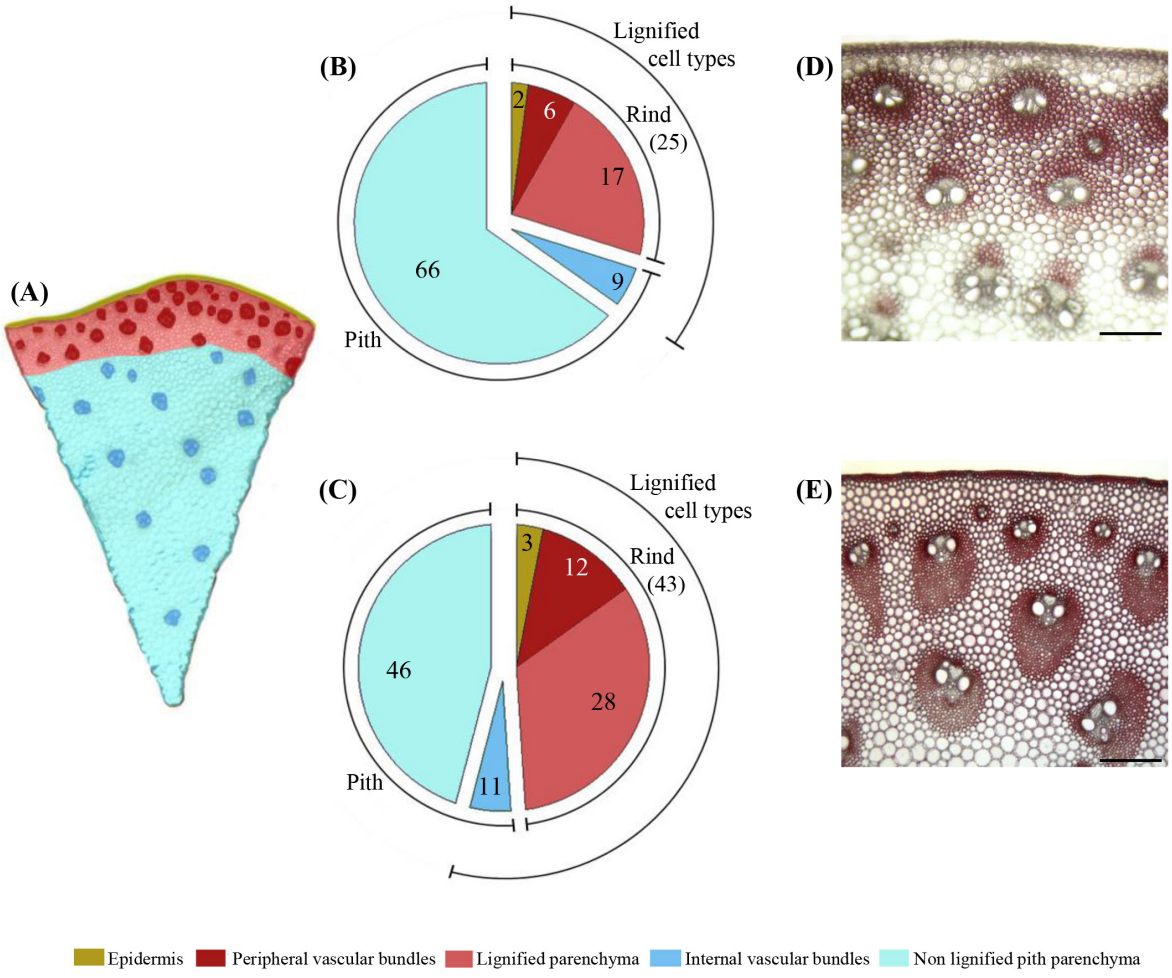

Figure 2 - Relative proportion of different cell types in Cm484 and F98902 internodes. **a**: Color-coded cell types of a typical internode cross section, the rind region (reddish color) containing closely packed VB is distinguishesd from the pith region(blue color) which contains sparce VB. **b** and **c**: Relative proportion (%) of the different cell types in internodes of Cm484 and F98902 lines, respectively. **d** and **e**: Focus on the rind portion of phloroglucinol-HCl stained INS cross section of Cm484 and F98902 respectively. 3 plants were collected and 2 portions of each internode sections have been measured. Bars: 200 μm

was equipped with a transparent knife edge aperture and a computer-controlled x/y sample stage. The 15x Schwarzschild IR objective and a 15x15 μm aperture were selected to record infrared spectra of parenchyma, PVS and SES cell. Spectra were obtained from cross sections (thickness: 10 μm) of INEs at flowering stage (Cm484 and F98902). Sections were pretreated with amylase and protease. The spectra were baseline corrected and normalized (unit vector normalization) according to Robert et al (2005).

Laser Capture Microdissection (LCM)

At flowering stage, INE of three plants for each line were fixed in 70% ethanol. The basal region was cut into 1/8 portions and one portion from each plant was randomly chosen to be rehydrated and cross-sectioned to 50-70 μm using the Leica VT 100S vibratome. Sections were mounted on metal-framed PEN (PolyEthylene Naphthalate) membrane slides (Arcturus, LCM0521). Samples were air-dried and kept until they were used for LCM. The dried samples were placed on the Arcturus XT™ microdissection system (Arcturus Bioscience), and brought into focus. CapSure® Macro LCM caps (MDS Analytical Technologies, LCM0211) were then placed over the cross-section. After focusing the section, PVS were delimited and first cut using the diode pumped solid-state UV laser (355 nm). This step had to be repeated at least three times to avoid contamination by surrounding cells when PVS were captured with the infrared laser. The following parameters were used: UV laser power = 100%, all filters out; UV cutting speed = 425; IR laser power = 65 mW. The amount of PVS captured represented an approximate surface area of 4 mm² for each line.

Results

Cm484 and F98902: two maize lines displaying contrasted digestibility and lignin chemistry

When grown under greenhouse conditions, Cm484 was significantly shorter at the flowering stage than F98902 (Table 1). This difference in height was mainly due to aerial internode number (15 in F98902 and 11 in Cm484). The diameter of the INE was similar in both lines. Cm484 flowered 15 days earlier than F98902.

Cell wall chemistry was carried out at the 7-leaf and flowering stages (Table 2). At the 7-leaf stage, no significant differences in digestibility between the two lines were observed. At flowering stage, the Cm484 INE was significantly more digestible than F98902 as indicated by higher IVNDFD (*In vitro* Neutral Detergent Fiber Digestibility) values. The lignin content of Cm484 INE was 3 points lower than that of F98902. Thioacidolysis indicated that Cm484 lignin was characterized by a high proportion of p-Hydroxyphenyl (H) units at both stages of development. At flowering stage, F98902 lignin was enriched in Syringyl (S) units compared to Cm484. Finally, ferulic acid content was not significantly different between the two

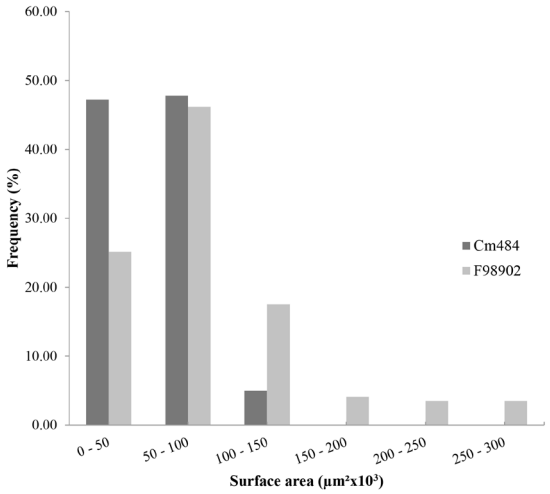

Figure 3 - Size distribution of VB in the rind parenchyma of Cm484 and F98902 internodes. 100μm thick cross-sections of INE collected at the flowering stage, were stained with pholoruglucinol and scanned. Surface area from 100 VB located in the rind parenchyma were measured using the Image PRO-Plus software (Media Cybernetics, Silver Spring, MD). Values for each class size are expressed as a percentage of the total VB.

lines at either developmental stage (data not shown). Quantification of the major cell wall monosaccharides showed that both lines contained less arabinose and galactose at flowering as compared to the 7-leaf stage (Supplementary Table 1). However, no significant differences in monosaccharides content were observed between Cm484 and F98902 at either stage of development.

In section cell wall degradability of internodes revealed more efficient fragmentation of Cm484 compared to F98902 tissues

At the whole plant level, cell wall chemistry and digestibility measurements showed clear differences between Cm484 and F98902 lines. In order to study cell type-specific dynamics of wall degradation, in section digestion assays with Celluclast enzyme were performed on INE at flowering stage (Figure 1). Within 24 h, no significant differences in tissue digestion were observed between the two lines (Figure 1b, f). The pith parenchyma separated from the rind and some of the internal vascular bundles became detached in F98902. After 48h (Figure 1c, g), the rind of Cm484 began to fragment (Figure 1c, see arrow) whereas the rind of F98902 remained intact. After 72h (Figure 1d, h), in Cm484 there were patches of rind parenchyma that were almost completely degraded, leaving only portions of the epidermis with SES and some vascular bundles undigested (Figure 1d see arrow). On the contrary, in F98902, the rind remained largely intact (Figure 1h). These results indicate a more extensive tissue fragmentation in Cm484 internodes compared to F98902.

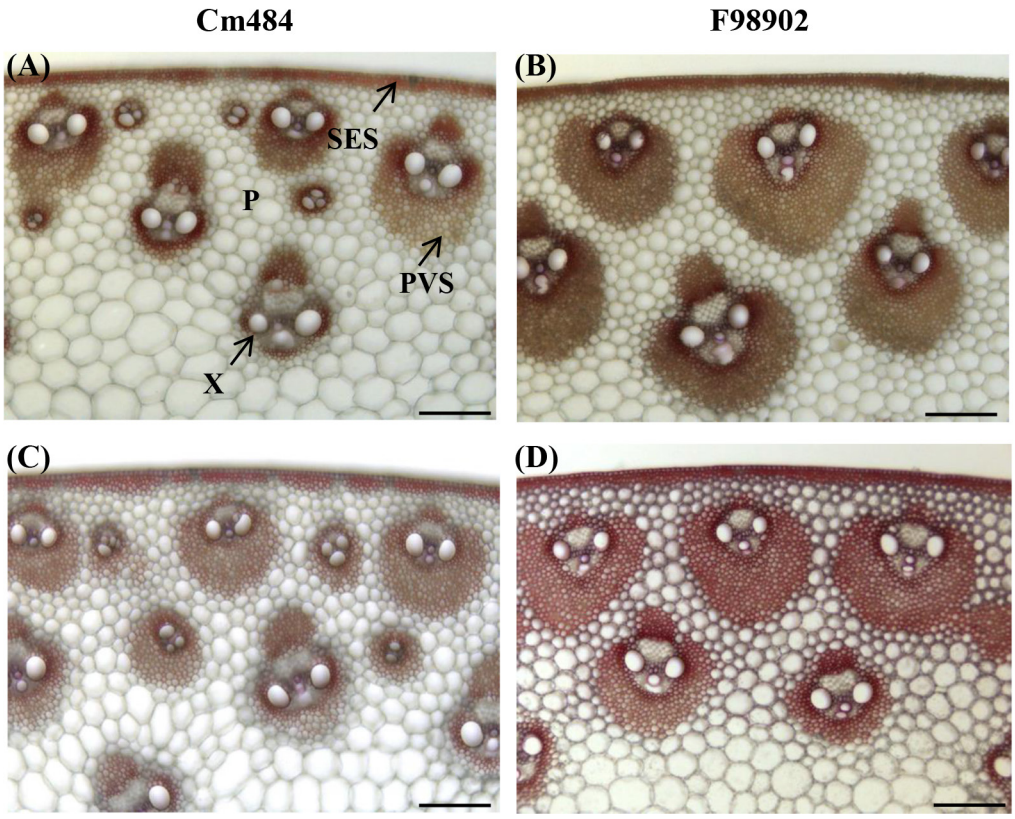

Figure 4 - Lignin staining of Cm484 and F98902 internodes at two developmental stages. **a** and **b**: 100μm thick cross section of Cm484 and F98902 respectively at flowering stage. **c** and **d**: 100μm thick cross section of Cm484 and F98902 at one month post-flowering stage. Phloroglucinol staining was performed on cross sections of INE from plants grown under greenhouse conditions at the flowering stage. The red color reveals the presence of lignin. P : Parenchyma, PVS : PeriVascular Sclerenchyma, SES : Sub-Epidermal Sclerenchyma, X : Xylem. Bars : 200 μm

Cell type patterning differs in internodes of Cm484 and F98902

To analyze cell type patterning in F98902 and Cm484 internodes, the relative surface area of the different cell types was quantified in the oldest internode, INS, where lignification was completed (Figure 2a-e). The total proportion of lignified cell types in the rind (parenchyma, peripheral vascular bundles and the epidermis) is significantly higher in F98902 than in Cm484 (43% vs. 25%, respectively). This is due to a greater proportion of lignified parenchyma and peripheral vascular bundles. These data prompted us to compare vascular bundle (VB) size and density within the rind. When considering peripheral VB size distribution, 95% were smaller than 100,000 µm^2 in Cm484 whereas in F98902, the size of VB was more variable, with a tendency towards larger bundles (≤ 300,000 µm^2) (Figure 3). Peripheral VB density was higher in Cm484 than in F98902, 1.6 and 0.9 VB mm^{-2} respectively. To further characterize peripheral VB, we measured cell wall thickness, cell density and the relative cell wall area of PVS. Interestingly, although the cell wall thickness was the same between F98902 and Cm484 (1.75 ± 0.34 µm vs 1.16 ± 0.35 µm), the cell density was greater in F98902 than in Cm484, 2,460 and 1,800 cells mm^{-2}, respectively. Consequently, this resulted in an overall greater relative proportion of cell wall surface area /total surface area in F98902 compared to Cm484, 0.57% and 0.33% respectively. Together, these results underline the significant differences in lignified cell type patterning between the two lines.

Delayed lignification and specific lignin composition of PVS (PeriVascular Sclerenchyma) between Cm484 and F98902

In order to follow the chronology of lignification of the different cell types, phloroglucinol-stained cross sections of Cm484 and F98902 INE were observed at the flowering stage and one month post-flowering (Figure 4). At the flowering stage, xylem vessels, SES and 1-3 PVS cell layers stained red with phloroglucinol in both lines (Figure 4a, b). One month later, a striking difference in the lignification pattern was observed between F98902 and Cm484. PVS was strongly stained in F98902 whereas in Cm484, only weak staining was observed (Figure 4c, d). At this stage, the rind parenchyma of F98902 was weakly lignified whereas it remained unlignified in Cm484.

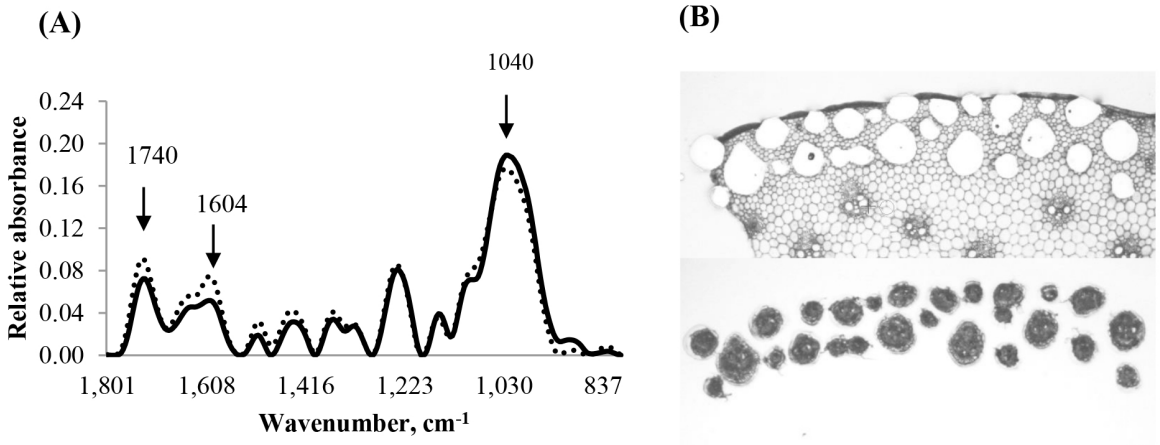

(C)

Line	Relative frequency of Thioacidolysis Monomers (Mol %)			S/G ratio
	H	G	S	
Cm484	7.37 ± 3.74	59.27 ± 1.94	33.36 ± 2.01	0.56 ± 0.02
F98902	2.05 ± 0.84	56.11 ± 1.96	41.04 ± 2.74	0.75 ± 0.07

Figure 5 - Lignin content and composition of PVS in Cm484 and F98902 lines. **a**: FTIR spectra of PVS. Peaks of interest, 1,604 cm^{-1} and 1,740 cm^{-1} representing lignins and 1,045 cm^{-1} representing xylans, are marked with arrows. Cm484 line is represented by full lines and F98902 by dotted lines. **b**: Laser capture microdissection of PVS. Isolation of PVS was carried out on 50 μm thick cross-sections using UV and IR laser beams. **c**: Thioacidolysis analysis of micro-dissected PVS. H, p-hydroxyphenyl; G, guaiacyl; S, syringyl. All experiments were performed on INE from three plants grown in greenhouse conditions and collected at the flowering stage.

Since several differences in PVS were observed between F98902 and Cm484 (ie greater surface area and cell density, difference in the timing of lignification), we subsequently focused our effort in characterizing this cell type at the cellular level. Fourier transform infrared (FTIR) microspectroscopy of PVS from Cm484 and F98902 indicated more lignin (wavelength: 1,604-1,740 cm^{-1}) and less xylan (wavelength: 1040 cm^{-1}) in F98902 than in Cm484 (Figure 5a). Thioacidolysis was then performed on laser capture micro-dissected PVS (Figure 5b). In PVS of Cm484, the lignin monomeric composition had a relatively higher proportion of H units whereas PVS of F98902 was more S-rich (Figure 5c). These results are in agreement with thioacidolysis data performed on whole INE, suggesting that the lignin composition and proportion of PVS influences global lignin composition in these two lines.

Differential expression of phenylpropanoid genes and associated Transcription Factors

To understand the mechanisms underlying the differences in cell wall chemistry and tissue patterning between F98902 and Cm484, transcriptomic analysis was performed on INE at flowering stage using the 18K Affymetrix Maize Genome Array. The complete data set is available at NCBI under accession GSE 18857. A total of 2,496 genes were differentially expressed between the two lines. 1,183 were up-regulated and 1,313 down-regulated in F98902 compared to Cm484. Differentially expressed genes associated with phenylpropanoid metabolism are shown in Figure 6. Upstream, genes including shikimate kinase, the entry point enzyme into the shikimate pathway and chorismate synthase, are more highly expressed in F98902, suggesting enhanced channelling of phenylpropanoid metabolites in this line. Further downstream in the phenylpropanoid pathway, Hydroxycinnamoyl-CoA Shikimate/Quinate Hycroxycinnamoyl Transferase (HCT), p-coumarate 3-hydroxylase CYP98A3 (C3H) and Caffeoyl-CoA 3-O-methyltransferase 1 (CCoAOMT1) from the

lignin branch of the pathway were more highly expressed in F98902 than in Cm484. Interestingly, all of these genes, were already up-regulated in F98902 at the 7-leaf stage (data not shown). Similarly, the expression of anthocyanin biosynthetic genes such as Chalcone isomerase (CHI) and Dihydroflavonol-4-reductase (DFR) was also up-regulated in F98902. Conversely, genes involved in flavonoid metabolism such as Flavonol Synthase (FLS) and Flavonoid 3'-monooxygenase (TT7) as well as Pinoresinol Reductase 1 (PLR), a key enzyme of lignan synthesis, were down-regulated in F98902.

Several TFs that regulate cell wall biosynthesis in different plant species have been reported (Zhong et al, 2011; Zhong et al, 2008). Among the most studied, R2R3-MYB TFs have been shown in some cases to be negative regulators of lignification (Fornalé et al, 2010; Fornalé et al, 2006; Sonbol et al, 2009). Eight MYB factors were differentially expressed between the two lines (Supplementary Table 2). Among them, three belonging to the R2R3-MYB family are significantly down-regulated in F98902. Upstream, NAC TFs are involved in fiber differentiation and secondary cell wall formation (Zhong et al, 2006; Zhong et al, 2007). Among the 18 NAC genes deposited on the 18K Affymetrix Maize Genome Array, one was up-regulated in Cm484 and one down-regulated. ANAC073 (SND2) which was down-regulated in Cm484 plays a role in secondary cell wall formation in Arabidopsis (Zhong et al, 2008). More recently, WRKY TFs which are normally associated with disease response have also been shown to be involved in the lignification of parenchyma cells in Arabidopsis (Wang et al, 2010). Three WRKYs were down-regulated in F98902 lines (Supplementary Table 2). Finally, 22 Zinc finger genes were differentially expressed in Cm484 vs. F98902 (Supplementary Table 2). In the plant kingdom, Zinc finger genes comprise a large family and play important roles in various physiological processes (Ciftci-Yilmaz and Mittler, 2008). In relation to cell wall formation, it has been shown that some Zinc finger proteins are up-regulated during the formation of tension wood in poplar (Andersson-Gunneras et al, 2006). Moreover, it has been shown that the family belonging to the CCCH type is the targets of WRKY TFs (Wang et al, 2010).

Discussion

Tissue fragmentation: a key step in cell wall degradability

Although cell wall digestibility in maize has been extensively studied over the past decades at the whole plant level, the current view of the different factors determining forage digestibility at cellular level remains fragmentary (Boon et al, 2005; Boon et al, 2008; Engels and Schuurmans, 1992; Jung and Casler, 2006; Lopez et al, 1993; Scobbie et al, 1993). In section digestibility studies presented herein show that, although the initial first steps of tissue degradation were indistinguishable between the two lines, cell wall degradation, independently of the inherent digestibility of the lines, does not appear to occur in a spatially random manner. In both genotypes, the pith parenchyma cells at the lignified/non lignified interface and the bundle sheath layer surrounding each inner vascular bundle were the first cell types to be degraded (Figure 1b, f). These results are in agreement with those obtained by (Jung and Casler, 2006) who analyzed the degradation in internode sections of three maize hybrids in the presence of rumen gastric fluid. This suggests that the cell wall degradation process is similar with commercial and ruminant microbial enzymes. The most striking differences between the two lines occurred at a later stage of degradation (72h) with a clear fragmentation of the rind in Cm484 compared to F98902 (Figure 1d, h). This could be related to differences in cell type patterning (higher sclerenchyma/parenchyma ratio in the peripheral rind of F98902), thereby limiting enzyme accessibility. In the future, it would be of interest to investigate the kinetics of in vitro enzyme adhesion to these different cell types in maize internodes.

Delayed lignification of PVS in Cm484 line is correlated with down-regulation of lignification genes and up-regulation of R2R3-MYB TFs

In maize, lignification is spatiotemporally regulated not only at the whole plant level, but also within a given internode (Guillaumie et al, 2007b; Scobbie et al, 1993). Moreover, at the cellular level, all cell types that are destined to lignify do not undergo lignification simultaneously or at the same rate (Joseleau and Ruel, 1997). For example, in maize internodes, vessels and fibers undergo secondary wall lignification earlier than parenchyma (Joseleau and Ruel, 1997). Herein, by combining cytological and biochemical approaches we show that the chronology of lignification of PVS is an important factor in discriminating Cm484 and F98902 lines. In Cm484, even one month after flowering, which corresponds to the harvest stage for silage maize, the PVS is only very weakly lignified compared to F98902. This result cannot be explained by differences in internode elongation since the delay in lignification was not systematically observed in all cell types. For example, SES was lignified to the same extent in Cm484 and F98902 internodes at both time points. Interestingly, laser capture micro-dissected PVS of Cm484 were more H unit-rich compared to F98902 PVS. Typically, H units are the first to be laid down, followed by G and then S units (Terashima et al, 1993). The fact that H units are proportionately more abundant in Cm484 suggests a more "juvenile" lignin in this line. In keeping with the lower lignin content and a delay in lignification in Cm484, transcriptomic data showed a down-regulation of HCT, C3H and CCoAOMT1 genes. These genes have previously been shown to be involved in G/S unit flux (Day et al, 2009; Nakashima et al, 2008). Moreover, three MYB factors were more highly expressed in Cm484 than in

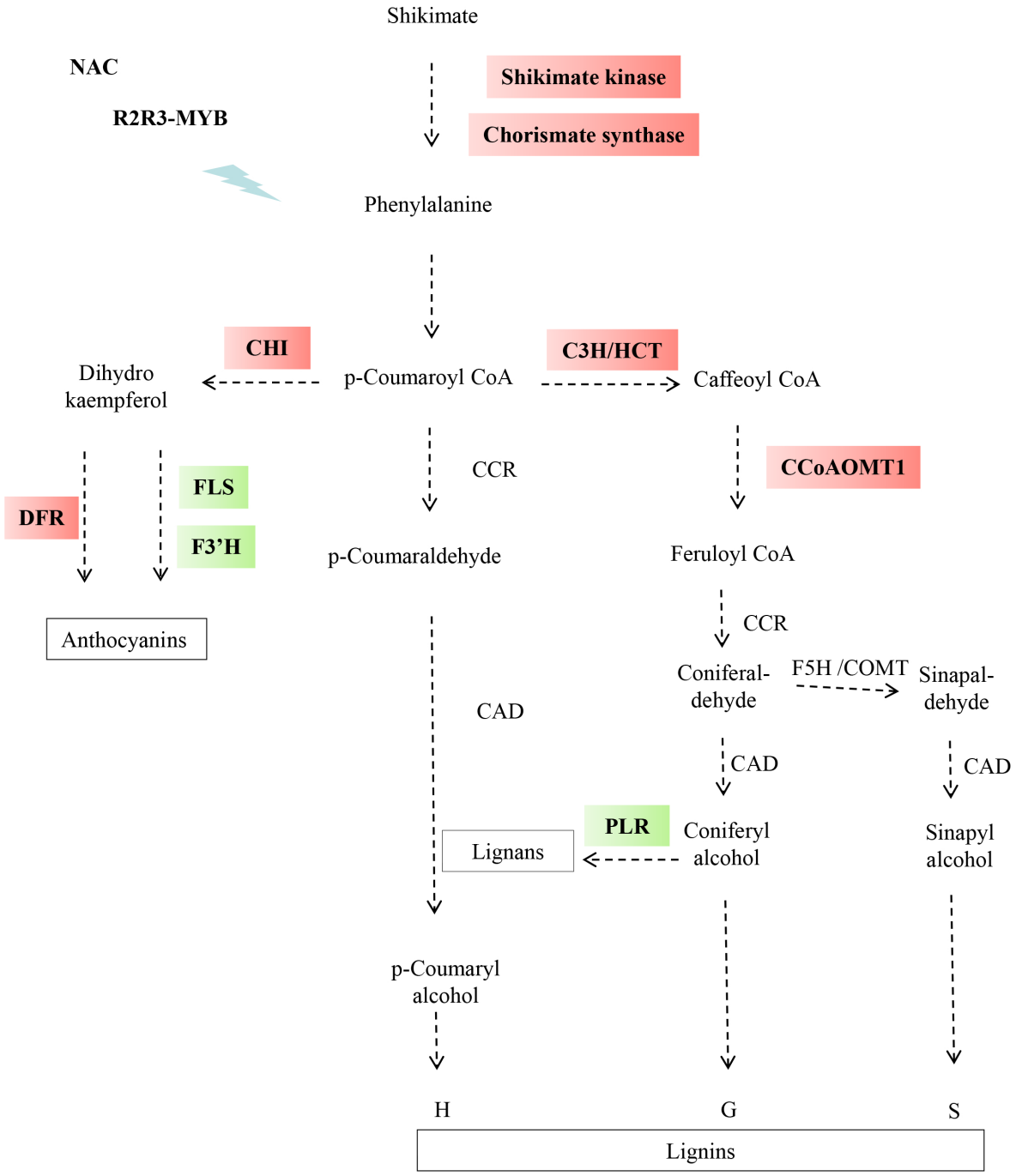

Figure 6 - Differential gene expression of shikimate and phenylpropanoid pathways in Cm484 and F98902 INEs. A decrease or increase in gene expression in F98902 is indicated by green or red boxes respectively. Shikimate kinase (AY105920.1), Chorismate synthase (AY105171.1), Hydroxycinnamoyl transferase (HCT1, CF045093) p-coumarate 3-hydroxylase (C3H, CO527025), Caffeoyl-CoA O-methyltransferase, (CCoAOMT1, AI691472), Chalcone isomerase (CHI, CD437816), Dihydroflavonol-4- reductase (DFR, BM073419), Flavonol Synthase (FLS, CO529883), Flavonoid 3'-monooxygenase (TT7 AY072297.1) and Pinoresinol Reductase 1 (PRR1, AW400260). RNA was extracted from 6 INEs collected at the flowering stage, and pooled into two samples for analysis.

F98902. These MYB genes belong to the R2R3-MYB factor family, whose members have been characterized as negative regulators of lignification (Fornalé et al, 2010; Sonbol et al, 2009). For example, the overexpression of the maize ZmMYB42 gene in Arabidopsis led to the down-regulation of several genes involved in lignin and flavonol biosynthesis (Sonbol et al, 2009). The overexpression of ZmMYB31 in Arabidopsis also resulted in the down-regulation of several genes along the monolignol biosynthetic pathway, whereas anthocyanin biosynthetic genes were induced (Fornalé et al, 2010). The expression pattern of R2R3-MYB factor and phenylpropanoid pathway genes in Cm484 is in keeping with these studies: three R2R3-MYB TFs were up-regulated, lignin and flavonoid biosynthetic genes were repressed, and genes involved in anthocyanin production induced. Thus, these three R2R3-MYB TFs, which are closely related but not identical to ZmMYB31 and ZmMYB42, represent new candidate genes for improving digestibility in maize.

Digestibility: more a complex developmental biologic process than just cell wall chemistry

Several studies on Arabidopsis mutants indicated that vascular cell type patterning is under genetic control (Fukuda, 2004). For example, the Arabidopsis mutant, *avb1* (*amphivasal vascular bundles*), exhibits a monocot instead of a dicot vascular architecture (Zhong et al, 1999). This gain of function mutation in IFL/REV, a class III HD-Zip gene, is essential for embryo patterning, meristem initiation and homeostasis, and vascular development (Zhong and Ye, 2004). In our studies, many lines of evidence converge towards differences in cell type patterning between Cm484 and F98902. They include i), vascular bundle organization in terms of both size and number, ii), rind parenchyma thickness, and iii), PVS cell density and hence the relative proportion of PVS cell wall- surface area/ total cell surface area. F98902 is characterized by fewer, yet larger vascular bundles whereas Cm484 contained numerous vascular bundles with proportionately less PVS. Interestingly, the mutation in the cell wall-related COBRA-like protein in the maize mutant, Brittle stalk2, resulted in changes in stem anatomy (Ching et al, 2006; Sindhu et al, 2007). The wild-type stems produce small VB similar to Cm484, whereas the bk2 resembled F98902. Similarly, Fornalé et al (2011) reported that transgenic maize plants down-regulated for CAD exhibited increased number of VB with less-developed sclerenchyma. Variations in vascular bundle number have also been reported in several rice mutants. One of them, nrl1, for narrow and rolled leaf mutant (Wu et al, 2010) is affected in a cellulose synthase-like D4 gene. Interestingly, in Cm484, one of the most down-regulated gene was a cellulose synthase-like D2 gene (see full dataset No accession GSE 18857). Another is *nal1*, for *narrow leaf gene* (Qi et al, 2008), mutated in a gene of unknown function, that provokes a severe defect in polar auxin transport. *nal1* culms exhibited an overall increase in VB number, especially in the peripheral ring, as well as an increase amount of parenchyma cells, reminiscent of the Cm484 lignified cell type patterning. Significant differences in the transcriptional regulation of hormone metabolism, and in particular auxin, were observed between the two lines (Supplementary Table 3), suggesting the importance of auxin signaling in cell type patterning in maize. Together, cytological and transcriptomic data suggest that digestibility should be considered in a developmental biologic context as opposed to just a cell wall context. It would be of interest to define the precise moment in plant development when lignified cell type patterning in maize is determined. This information could facilitate the identification of QTLs (and their underlying genes) that control the proportion of lignified tissues, vascular bundle size and number as a novel approach to improving cell wall digestibility in maize.

Acknowledgements

This work was supported by the Association Interprofessionnelle du Développement des Semences du Sud-Ouest, the Institut National de la Recherche Agronomique and the Centre National de la Recherche Scientifique. We would like to thank the people from Biogemma and Syngenta greenhouses, Michel Pagniez, Fabienne Mezzasalma and Sylvie Loras, and Véronique Rois respectively. We also sincerely thank Frédéric Legée and Laurent Cézard (UMR 1318 AgroParisTech-INRA) for the lignin analysis. The LCM equipment was financed by the Region Midi-Pyrénées.

References

Andersson-Gunneras S, Mellerowicz EJ, Love J, Segerman B, Ohmiya Y, Coutinho PM, Nilsson P, Henrissat B, Moritz T, Sundberg B, 2006. Biosynthesis of cellulose-enriched tension wood in Populus: global analysis of transcripts and metabolites identifies biochemical and developmental regulators in secondary wall biosynthesis. Plant J 45: 144-165

Barrett T, Troup DB, Wilhite SE, Ledoux P, Rudnev D, Evangelista C, Kim IF, Soboleva A, Tomashevsky M, Edgar R, 2007. NCBI GEO: mining tens of millions of expression profiles--database and tools update. Nucleic Acids Res (Database issue) 35: D760-765

Beaugrand J, Cronier D, Thiebeau P, Schreiber L, Debeire P, Chabbert B, 2004. Structure, chemical composition, and xylanase degradation of external layers isolated from developing wheat grain. J Agric Food Chem 52: 7108-7117

Boon EJMC, Engels FM, Struik PC, Cone JW, 2005. Stem characteristics of two forage maize (*Zea mays* L) cultivars varying in whole plant digestibility. II. Relation between *in vitro* rumen fermenta-

tion characteristics and anatomical and chemical features within a single internode. Njas-Wagen J Life Sc 53: 87-109

Boon JJ, Struik PC, Tamminga S, Engels FM, Cone JW, 2008. Stem characteristics of two forage maize (*Zea mays* L) cultivars varying in whole plant digestibility. III. Intra-stem variability in anatomy, chemical composition and in vitro rumen fermentation. NJAS 56: 101-122

Cherney DJR, Mertens DR, Moore JE, 1990. Morphology, fiber composition and mean particle diameter relationships in ground barley and oat forages at different ages. Anim Feed Sci Tech 31: 65-78

Ching A, Dhugga KS, Appenzeller L, Meeley R, Bourett TM, Howard RJ, Rafalski A, 2006. Brittle stalk 2 encodes a putative glycosylphosphatidylinositol-anchored protein that affects mechanical strength of maize tissues by altering the composition and structure of secondary cell walls. Planta 224: 1174-1184

Ciftci-Yilmaz S, Mittler R, 2008. The zinc finger network of plants. Cell Mol Life Sci 65: 1150-1160

Cossegal M, Chambrier P, Mbelo S, Balzergue S, Martin-Magniette ML, Moing A, Deborde C, Guyon V, Perez P, Rogowsky P, 2008. Transcriptional and metabolic adjustments in ADP-glucose pyrophosphorylase-deficient bt2 maize kernels. Plant Physiol 146: 1553-1570

Courtial A, Jourda C, Arribat S, Balzergue S, Huguet S, Reymond M, Grima-Pettenati J, Barrière Y, 2012. Comparative expression of cell wall related genes in four maize RILs and one parental line of variable lignin content and cell wall degradability. Maydica 57: 56-74

Day A, Neutelings G, Nolin F, Grec S, Habrant A, Cronier D, Maher B, Rolando C, David H, Chabbert B, Hawkins S, 2009. Caffeoyl coenzyme A O-methyltransferase down-regulation is associated with modifications in lignin and cell-wall architecture in flax secondary xylem. Plant Physiol Biochem 47: 9-19

Dembinsky D, Woll K, Saleem M, Liu Y, Fu Y, Borsuk LA, Lamkemeyer T, Fladerer C, Madlung J, Barbazuk B, Nordheim A, Nettleton D, Schnable PS, Hochholdinger F, 2007. Transcriptomic and proteomic analyses of pericycle cells of the maize primary root. Plant Physiol 145: 575-588

Engels FM, Schuurmans JLL, 1992. Relationship between structural development of cell-walls and degradation of tissues in maize stems. J Sci Food Agr 59: 45-51

Fornalé S, Capellades M, Encina A, Wang K, Irar S, Lapierre C, Ruel K, Joseleau JP, Berenguer J, Puigdomènech P, Rigau J, Caparrós-Ruiz D, 2011. Altered lignin biosynthesis improves cellulosic bioethanol production in transgenic maize plants down-regulated for cinnamyl alcohol dehydrogenase. Mol Plant 5: 817-830

Fornalé S, Shi X, Chai C, Encina A, Irar S, Capellades M, Fuguet E, Torres JL, Rovira P, Puigdomenech P, Rigau J, Grotewold E, Gray J, Caparros-Ruiz D, 2010. ZmMYB31 directly represses maize lignin genes and redirects the phenylpropanoid metabolic flux. Plant J 64: 633-644

Fornalé S, Sonbol FM, Maes T, Capellades M, Puigdomenech P, Rigau J, Caparros-Ruiz D, 2006. Down-regulation of the maize and Arabidopsis thaliana caffeic acid O-methyl-transferase genes by two new maize R2R3-MYB transcription factors. Plant Mol Biol 62: 809-823

Fukuda H, 2004. Signals that control plant vascular cell differentiation. Nat Rev Mol Cell Bio 5: 379-391

Gagnot S, Tamby JP, Martin-Magniette ML, Bitton F, Taconnat L, Balzergue S, Aubourg S, Renou JP, Lecharny A, Brunaud V, 2008. CATdb: a public access to Arabidopsis transcriptome data from the URGV-CATMA platform. Nucleic Acids Res (Database issue) 36: D986-990

Goto M, Morita O, Chesson A, 1991. Morphological and anatomical variations among barley cultivars influence straw degradability. Crop Sci 31: 1536-1541

Guillaumie S, Pichon M, Martinant JP, Bosio M, Goffner D, Barrière Y, 2007a. Differential expression of phenylpropanoid and related genes in brown-midrib bm1, bm2, bm3, and bm4 young near-isogenic maize plants. Planta 226: 235-250

Guillaumie S, San-Clemente H, Deswarte C, Martinez Y, Lapierre C, Murigneux A, Barrière Y, Pichon M, Goffner D, 2007b. MAIZEWALL. Database and developmental gene expression profiling of cell wall biosynthesis and assembly in maize. Plant Physiol 143: 339-363

Joseleau JP, Ruel K, 1997. Study of lignification by noninvasive techniques in growing maize internodes. An investigation by Fourier transform infrared cross-polarization-magic angle spinning 13C-nuclear magnetic resonance spectroscopy and immunocytochemical transmission electron microscopy. Plant Physiol 114: 1123-1133

Jung HG, Casler MD, 2006. Maize stem tissues: Impact of development on cell wall degradability. Crop Sci 46: 1801-1809

Lopez S, Murison SD, Travis AJ, Chesson A, 1993. Degradability of parenchyma and sclerenchyma cell-walls isolated at different developmental stages from a newly extended maize internode. Acta Bot Neerl 42: 165-174

McCann MC, Defernez M, Urbanowicz BR, Tewari JC, Langewisch T, Olek A, Wells B, Wilson RH, Carpita NC, 2007. Neural network analyses of infrared spectra for classifying cell wall architectures. Plant Physiol 143: 1314-1326

Méchin V, Argillier O, Rocher F, Hébert Y, Mila I, Pollet B, Barrière Y, Lapierre C, 2005. In search of a maize ideotype for cell wall enzymatic degradabil-

ity using histological and biochemical lignin characterization. J Agric Food Chem 53: 5872-5881

Migné C, 1995. Localisation immunocytochimique des constituants pariétaux de l'entre-noeud apical de la tige de maïs avant et après dégradation dans le rumen. Thèse Université Blaise Pascal, Clermont-Ferrand

Mouille G, Robin S, Lecomte M, Pagant S, Hofte H, 2003. Classification and identification of Arabidopsis cell wall mutants using Fourier-Transform InfraRed (FT-IR) microspectroscopy. Plant J 35: 393-404

Nakano J, Meshitsuka G, 1992. The detection of lignin, pp 23-61. In: Methods in lignin chemistry. Lin SY, Dence CW eds. Springer-Verlag, Berlin

Nakashima J, Chen F, Jackson L, Shadle G, Dixon RA, 2008. Multi-site genetic modification of monolignol biosynthesis in alfalfa (*Medicago sativa*): effects on lignin composition in specific cell types. New Phytol 179: 738-750

Nakazono M, 2003. Laser-Capture Microdissection, a tool for the global analysis of gene expression in specific plant cell types: Identification of genes expressed differentially in epidermal cells or vascular tissues of maize. Plant Cell 15: 583-596

Qi J, Qian Q, Bu Q, Li S, Chen Q, Sun J, Liang W, Zhou Y, Chu C, Li X, Ren F, Palme K, Zhao B, Chen J, Chen M, Li C, 2008. Mutation of the rice *Narrow leaf1* gene, which encodes a novel protein, affects vein patterning and polar auxin transport. Plant Physiol 147: 1947-1959

Robert P, Marquis M, Barron C, Guillon F, Saulnier L, 2005. FT-IR investigation of cell wall polysaccharides from cereal grains. Arabinoxylan infrared assignment. J Agric Food Chem 53: 7014-7018

Ruel K, Berrio-Sierra J, Derikvand MM, Pollet B, Thevenin J, Lapierre C, Jouanin L, Joseleau JP, 2009. Impact of CCR1 silencing on the assembly of lignified secondary walls in *Arabidopsis thaliana*. New Phytol 184: 99-113

Schertz KF, Rosenow DT, 1977. Anatomical variation in stalkinternodes of sorghum. Crop Sci 17: 628-631

Scobbie L, Russell W, Provan GJ, Chesson A, 1993. The newly extended maize internode: a model for the study of secondary cell wall formation and consequences for digestibility. J Sci Food Agric 61: 217-225

Sindhu A, Langewisch T, Olek A, Multani DS, McCann MC, Vermerris W, Carpita NC, Johal G, 2007. Maize Brittle stalk2 encodes a COBRA-like protein expressed in early organ development but required for tissue flexibility at maturity. Plant Physiol 145: 1444-1459

Sonbol FM, Fornale S, Capellades M, Encina A, Tourino S, Torres JL, Rovira P, Ruel K, Puigdomenech P, Rigau J, Caparros-Ruiz D, 2009. The maize ZmMYB42 represses the phenylpropanoid pathway and affects the cell wall structure, composition and degradability in *Arabidopsis thaliana*. Plant Mol Biol 70: 283-296

Tamasloukht B, Wong Quai Lam MS, Martinez Y, Tozo K, Barbier O, Jourda C, Jauneau A, Borderies G, Balzergue S, Renou JP, Huguet S, Martinant JP, Tatout C, Lapierre C, Barrière Y, Goffner D, Pichon M, 2011. Characterization of a *cinnamoyl-CoA reductase 1* (*CCR1*) mutant in maize: effects on lignification, fibre development, and global gene expression. J Exp Bot 62: 3837-3848

Terashima N, Fukushima K, He LF, Takabe K, 1993. Comprehensive model of the lignified plant cell wall, pp. 133–163. In: Cell Wall Structure and Digestibility. Ralph J ed. American Society of Agronomy Inc, Madison, WI

Thomas J, Guillaumie S, Verdu C, Denoue D, Pichon M, Barrière Y, 2010. Cell wall phenylpropanoid-related gene expression in early maize recombinant inbred lines differing in parental alleles at a major lignin QTL position. Mol Breeding 25(1): 105-124

Twidwell EK, Johnson KD, Patterson JA, Cherney JH, Bracker CE, 1990. Degradation of switchgrass anatomical tissue by rumen microorganisms. Crop Sci 30: 1321-1328

Wang H, Avci U, Nakashima J, Hahn MG, Chen F, Dixon RA, 2010. Mutation of WRKY transcription factors initiates pith secondary wall formation and increases stem biomass in dicotyledonous plants. Proc Natl Acad Sci USA 107: 22338-22343

Wilson JR, 1993. Isolates of cell types from sorghum stems: Digestion, cell wall and anatomical characteristics. J Sci Food Agric 63: 407-417

Wu C, Fu Y, Hu G, Si H, Cheng S, Liu W, 2010. Isolation and characterization of a rice mutant with narrow and rolled leaves. Planta 232: 313-324

Zhong R, Demura T, Ye ZH, 2006. SND1, a NAC domain transcription factor, is a key regulator of secondary wall synthesis in fibers of Arabidopsis. Plant Cell 18: 3158-3170

Zhong R, Lee C, McCarthy RL, Reeves CK, Jones EG, Ye ZH, 2011. Transcriptional activation of secondary wall biosynthesis by rice and maize NAC and MYB transcription factors. Plant Cell Physiol 52: 1856-1871

Zhong R, Lee C, Zhou J, McCarthy RL, Ye ZH, 2008. A battery of transcription factors involved in the regulation of secondary cell wall biosynthesis in Arabidopsis. Plant Cell 20: 2763-2782

Zhong R, Richardson EA, Ye ZH, 2007. Two NAC domain transcription factors, SND1 and NST1, function redundantly in regulation of secondary wall synthesis in fibers of Arabidopsis. Planta 225: 1603-1611

Zhong R, Ye ZH, 2004. Amphivasal vascular bundle 1, a gain-of-function mutation of the *IFL1/REV* gene, is associated with alterations in the polarity of leaves, stems and carpels. Plant Cell Physiol 45: 369-385

Zhong RQ, Taylor JJ, Ye ZH, 1999. Transformation of the collateral vascular bundles into amphivasal vascular bundles in an Arabidopsis mutant. Plant Physiol 120: 53-64

Supplementary Table 1: Relative frequency of different sugar monomers recovered from acid hydrolysis of Cm484 and F98902 internodes at two developmental stages. The mean values and standard deviations have been calculated from measurements on 6 plants. Arabinose (ARA), Galactose (GAL), Glucose (GLC) and Xylose (XYL).

Stage and samples	Lines	ARA	GAL	GLC	XYL
		%			
Piled-up internodes at the 7- leaf stage	Cm484	6.75 ± 0.26	1.58 ± 0.09	59.45 ± 0.28	33.23 ± 1.34
	F98902	8.00 ± 0.55	2.70 ± 0.30	53.52 ± 1.35	35.78 ± 0.49

Supplementary Table 2: Differential expression of Transcription Factors (TFs) between Cm484 and F98902 lines. Experiments were performed with RNA extracted from INE pooled from 6 plants.

Gene	Accession N°	Log2 ratio	Bonferonni
TFs			
Down-regulated genes in F98902			
Myb TFs			
AtMYB36 homolog (ZmMYBHX22 R 2R3-MYB)	gb|AF099381.1	-4,61	0,00E+00
AtMYB59-3 homolog (ZmMYBIM65 R2R3-MYB)	gb|AF099413.1	-3,31	0,00E+00
AtMYB60 homolog (ZmMYBIM61 R2R3-MYB)	gb|AF099412.1	-2,04	0,00E+00
NAC TFs			
ANAC073 (Arabidopsis NAC Domain Containing Protein 73)	gb|CF045441	-2,28	0,00E+00
WRKY TFs			
AtWRKY3 homolog	gb|AI770340	-1,79	7,65E-11
AtWRKY2 homolog	gb|CF629057	-1,65	8,84E-09
AtWRKY21 homolog	gb|CO520243	-1,28	4,01E-04
Zinc finger TFs			
zinc finger (GATA type) family protein	gb|BM380250	-3,99	0,00E+00
zinc finger (CCCH-type) family protein	gb|AY108495.1	-3,91	0,00E+00
zinc finger (C3HC4-type RING finger) family protein	gb|AI586583	-3,20	0,00E+00
zinc finger (C3HC4-type RING finger) family protein	gb|CO526259	-3,12	0,00E+00
MIF2 (Mini Zinc Finger 2)	gb|BM268263	-2,76	0,00E+00
zinc finger (C3HC4-type RING finger) family protein	gb|BQ539187	-2,72	0,00E+00
zinc finger (B-box type) family protein	gb|AY111725.1	-1,78	9,94E-11
LZF1 (Light-Regulated Zinc Finger Protein 1)	gb|BE051683	-1,57	9,67E-08
zinc finger (CCCH type) family protein	gb|BM080212	-1,56	1,41E-07
zinc finger (C3HC4-type RING finger) family protein	gb|BM078620	-1,27	4,32E-04
zinc finger (CCCH-type) family protein	gb|CA402806	-1,22	1,67E-03
Miscellaneous TFs			
AG (Agamous)	gb|L46399.1	-5,99	0,00E+00
SEP1 (Sepallata1)	gb|CO526301	-5,83	0,00E+00
SHP2 (Shatterproof 2)	gb|X85334.1	-3,95	0,00E+00
SHP2 (Shatterproof 2)	gb|X85335.1	-3,24	0,00E+00
bZIP family transcription factor	gb|CA404309	-2,36	0,00E+00
bHLH093 (beta HLH protein 93)	gb|AW146792	-2,19	0,00E+00
transducin family protein / WD-40 repeat family protein	gb|CF012473	-1,99	0,00E+00
E2F transcription factor 3	gb|CO530334	-1,62	2,45E-08
Transcription factor	gb|AI948165	-1,58	7,87E-08
AtBZIP9 homolog	gb|AY110737.1	-1,53	3,38E-07
ABF4 (ABRE binding factor 4)	gb|BM079714	-1,51	6,76E-07
YABBY 3	gb|BE644445	-1,40	1,71E-05
KNAT1	gb|AY107753.1	-1,38	2,30E-05
bHLH093	gb|CF016461	-1,29	3,09E-04

AtHB-1 homolog	gb|CK985510	-1,27	4,04E-04
bHLH family protein	gb|AY108831.1	-1,23	1,19E-03
bHLH family protein	gb|BG840791	-1,21	2,11E-03
AtHB-15 homolog	gb|AW066833	-1,20	2,54E-03
bHLH family protein	gb|CF632030	-1,19	2,85E-03
YABBY 5	gb|BF728921	-1,19	3,02E-03
bHLH071	gb|AI666008	-1,07	4,50E-02
CDF2 (Cycling DOF Factor 2)	gb|CO524637	-2,22	0,00E+00
TT8 (Transparent Testa 8)	gb|X57276.1	-2,19	0,00E+00
ATRL6 (Arabidopsis RAD-Like 6)	gb|BM381057	-1,83	1,91E-11
STY1 (Stylish 1)	gb|CO520087	-1,77	1,57E-10
AGAMOUS-LIKE 20	gb|AI491392	-1,71	1,12E-09
NF-YB3 (Nuclear factor Y, subunit B3)	gb|CA403909	-1,63	1,39E-08
WLIM1	gb|BM333846	-1,44	5,11E-06
AtBPC2 (Basic pentacysteine 2)	gb|AI600800	-1,34	6,65E-05
AP1 (Apetala 1)	gb|L46400.1	-1,20	2,68E-03
AGL22 | SVP (Short vegetative phase)	gb|AJ430635.1	-1,13	1,15E-02
Up-regulated genes in F98902			
Myb TFs			
AtMYB4 homolog	gb|CK370725	1,15	8,21E-03
AtMYB15 homolog	gb|CK369414	1,57	1,05E-07
Myb family transcription factor homolog	gb|BM075490	1,88	3,82E-12
AtMYB7 homolog	gb|CK368011	2,40	0,00E+00
AtMYB4 homolog	gb|CO524780	2,42	0,00E+00
NAC TFs			
AtNAC2 homolog	gb|BM380633	1,88	3,82E-12
WRKY TFs			
AtWRKY50 homolog	gb|BM334368	3,70	0,00E+00
Zinc finger TFs			
zinc finger (C3HC4-type RING finger) family protein	gb|CO533021	1,08	4,20E-02
zinc finger and C2 domain protein	gb|CD947211	1,15	7,78E-03
zinc finger (B-box type) family protein	gb|CK368046	1,19	2,87E-03
zinc finger (GATA type) family protein	gb|CO530177	1,82	2,68E-11
zinc finger (AN1-like) family protein	gb|CK370651	1,83	1,91E-11
zinc finger (C3HC4-type RING finger) family protein	gb|AI714503	1,84	1,15E-11
zinc finger (AN1-like) family protein	gb|CK370651	2,55	0,00E+00
zinc finger (DHHC type) family protein	gb|CD996768	3,03	0,00E+00
zinc finger (C3HC4-type RING finger) family protein	gb|BE051646	3,27	0,00E+00
zinc finger (FYVE type) family protein	gb|CD484576	3,27	0,00E+00
zinc finger (C3HC4-type RING finger) family protein	gb|BM351647	4,84	0,00E+00
Miscellaneous TFs			
AtMYC2 homolog	gb|AF061107.1	1,07	4,36E-02
COL2 (Contans-Like 2)	gb|AY105193.1	1,17	4,65E-03
SIGC (RNA Polymerase sigma-subunit C)	gb|AY091464.1	1,20	2,75E-03
AHBP-1B	gb|X69152.1	1,21	2,21E-03
WD-40 repeat family protein	gb|AI738295	1,21	1,82E-03
PFT1 (Phytochrome and Flowering Time 1)	gb|BG874087	1,31	1,87E-04
AtSIG2 (RNA Polymerase sigma subunit 2)	gb|AF099110.1	1,32	1,26E-04
AP1 (Apetala 1)	gb|AF112150.1	1,34	8,09E-05
LUG (Leunig)	gb|CA401505	1,36	4,74E-05

AtHB6 homolog	gb|AI734516	1,38	2,26E-05
NF-YA6	gb|AW061641	1,41	1,23E-05
AGL12 (Agamous-Like 12)	gb|CK348099	1,43	7,27E-06
Transcriptional factor B3 family protein	gb|CF635301	1,43	6,96E-06
WD-40 repeat family protein	gb|AW091209	1,48	1,68E-06
SNF2 domain-containing protein	gb|AI665143	1,51	6,94E-07
Transcription factor	gb|CF034955	1,57	9,63E-08
AHBP-1B	gb|X69152.1	1,65	7,50E-09
SPL12 (squamosa promoter-binding protein-like 12)	gb|AI461494	1,67	3,83E-09
RAP2.12	gb|CF626555	1,69	2,70E-09
AtBZIP9 homolog	gb|AY108582.1	1,88	3,82E-12
AP2 domain-containing transcription factor	gb|AY672654.1	2,38	0,00E+00
bHLH family protein	gb|BM380514	2,78	0,00E+00
BIM2 (BES1-interacting Myc-like protein 2)	gb|BG841113	2,91	0,00E+00
PCL1 (Phytoclock 1)	gb|BM269011	3,08	0,00E+00
Transcription factor jumonji domain-containing protein	gb|CO523709	3,41	0,00E+00
RAP2.4 (related to AP2 4)	gb|AY104042.1	3,36	0,00E+00
bZIP transcription factor family protein	gb|CK144438	5,13	0,00E+00

Supplementary Table 3: Differential expression of hormone metabolism between Cm484 and F98902 lines. Experiments were performed with RNA extracted from INE pooled from 6 plants.

Gene	Accession N°	Log2 ratio	Bonferonni
Hormone signalling pathway			
Down-regulated genes in F98902			
Auxin			
Auxin-responsive protein-related	gb|CO531270	-1,79	6,88E-11
ILR3 (IAA-Leucine Resistant 3)	gb|BM078135	-1,67	4,39E-09
ILR1 (IAA-Leucine Resistant 1)	gb|CO522313	-1,55	1,97E-07
ARF6 (Auxin-response factor 6)	gb|BM073969	-1,33	8,73E-05
Auxin-responsive protein-related	gb|AI691183	-1,22	1,46E-03
ARF3 (Auxin-response factor 3)	gb|BE638786	-1,19	3,27E-03
Ethylene			
EIN2	gb|CA402979	-4,16	0,00E+00
Giberellin			
gibberellin-regulated family protein	gb|AY108847.1	-2,37	0,00E+00
gibberellin-regulated family protein	gb|AY109960.1	-2,13	0,00E+00
GA20OX2 (Gibberellin 20 Oxidase 2)	gb|AY105651.1	-1,21	1,97E-03
GA2OX1 (Gibberellin 2-Oxidase 1)	gb|AY104425.1	-1,15	9,06E-03
ABA			
Abscisic acid-responsive HVA22 family protein	gb|CF009268	-2,35	0,00E+00
ABA-responsive protein-related	gb|BQ538711	-1,59	6,25E-08
ABF3 (Abscisic Acid Responsive Elements-Binding Factor 3)	gb|BG842791	-1,57	9,59E-08
Jasmonic acid			
JMT (Jasmonic Acid Carboxyl Methyltransferase)	gb|CF626198	-1,65	7,60E-09
JAZ12 (Jasmonate-ZIM-Domain Protein 12)	gb|BQ539591	-1,10	2,47E-02
Up-regulated genes in F98902			
Auxin			
IAA16	gb|BM350512	1,32	1,21E-04
AUX2-11	gb|BM347935	1,34	8,12E-05
AXR3 (Auxin Resistant 3)	gb|BM348544	1,37	3.59E-5E
ARF1 (Auxin Response Factor 1)	gb|AI834525	1,43	6,64E-06
IAA16	gb|CF623876	1,87	3,82E-12
IBR5 (Indole-3-Butyric Acid Response 5)	gb|AY108971.1	2,14	0,00E+00
ILR3 (iaa-leucine resistant3)	gb|BG841716	2,17	0,00E+00
AUX2-11	gb|BM268818	3,72	0,00E+00
Ethylene			
ERF-1 (Ethylene responsive element binding factor 1)	gb|BM348921	1,92	0,00E+00
Jasmonic acid			

JAZ1 (Jasmonate-ZIM-Domain Protein 1)	gb|BE512131	1,99	0,00E+00
JAZ1 (Jasmonate-ZIM-Domain Protein 1)	gb|BM074538	4,03	0,00E+00
Cytokinin			
ARR3 (*Arabidopsis* response regulator 3)	gb|AB004882.1	2,14	0,00E+00
ARR9 (*Arabidopsis* response regulator 9)	gb|AB042268.1	2,95	0,00E+00